RSC Advances

ROYAL SOCIETY OF CHEMISTRY

www.rsc.org/advances

Tunable band gap and magnetism of the two-dimensional nickel hydroxide

Zhen-Kun Tang[1,2], Wei-Wei Liu[1], Deng-Yu Zhang[2], Woon-Ming Lau[1,3], Li-Min Liu[1]*

[1] Beijing Computational Science Research Center, Beijing 100084, China
[2] College of Physics and Electronics Engineering, Hengyang Normal University, Hengyang 421008, China
[3]Chengdu Green Energy and Green Manufacturing Technology R&D Center, Chengdu, Sichuan, 610207, China

Email: limin.liu@csrc.ac.cn

Abstract: The electronic structures and magnetic properties of two dimensional (2D) hexagonal $Ni(OH)_2$ are explored based on first-principles calculations. The results reveal that the ground state of the pristine $Ni(OH)_2$ is a direct semiconductor with antiferromagnetic (AFM) coupling between two nearest Ni atoms. Interestingly, the monolayer $Ni(OH)_2$ becomes ferromagnetic (FM) semiconductor under a biaxial compressive strain of 4%. Furthermore, both the band gap and direct-indirect gap transition of monolayer $Ni(OH)_2$ can be modulated by the different biaxial strains. These tunable electronic structures and magnetic properties of the monolayer $Ni(OH)_2$ make it promising candidate for applications in 2D spin-devices.

1. Introduction

In the past ten years, two-dimensional (2D) layered materials have received tremendous attention due to the unusual physical and chemical properties[1-10]. Graphene is the most famous 2D material,[11-14] which has many superior properties such as remarkable Young's modulus, tremendous electrical conductivity, and excellent thermal conductivity. Unfortunately, the magnetic property is absent in pristine 2D graphene materials, which greatly hamper its application in spintronic device[15]. Several approaches of introducing magnetism to graphene, such as vacancy[16], defect[17] and edge effect of nanoribbons[18], have been examined. However, the introduction of uniformly defective graphene is rather complicated, and the precise manipulation of these defects is still challenging. Thus, it is greatly desirable to search some novel 2D materials with the intrinsic magnetism for 2D spintronic device. Recent theoretical studies indicate that several monolayer transition-metal dichalcogenides, such as VX_2[19, 20] (X=S, Se) and MnX_2[21, 22] (X=O, S, Se), own intrinsic ferromagnetism in the pristine layered structures. Recently, the room temperature ferromagnetism of the ultrathin VS_2 nanosheets are detected by experimental measurements[23].

Nickel hydroxide ($Ni(OH)_2$) is widely used in alkaline rechargeable batteries[24, 25] and supercapacitors[26, 27]. Experimentally, hexagonal ultrathin $Ni(OH)_2$ nanosheets have synthesized by exfoliation of layered nickel hydroxides[28] or simple electrochemical reaction[29]. However, the detailed electronic properties of such monolayer $Ni(OH)_2$ have not been investigated by the first-principles calculations. Considering the partially filled 3d shells of the Nickel (Ni) atom, the monolayer $Ni(OH)_2$ may exhibit special spin polarization and magnetic coupling. The recent experimental result shows that $Ni(OH)_2$ nanosheet has an antiferromagnetic (AFM) order without macro magnetic moment[30, 31], which limits its direct application for 2D spin-based devices. It is well known that the adjustable magnetism is crucial for the relatively novel field of spintronics[32]. Several groups have reported the strain-controlled magnetism in pristine 2D materials[19, 33-35]. Thus, the unusual electronic and magnetic properties of the pristine monolayer $Ni(OH)_2$ may exist under the strain condition.

In this work, first-principles calculations were carried out to systematically examine the stability, electronic structure, and magnetic properties of the hexagonal monolayer $Ni(OH)_2$. Phonon spectrum analysis shows that the monolayer $Ni(OH)_2$ is thermodynamically stable. The ground state of the monolayer $Ni(OH)_2$ is antiferromagnetic semiconductor with a direct band gap. Interestingly, the magnetism of the monolayer $Ni(OH)_2$ can transform into ferromagnetic under a biaxial compressive strain, and the magnetic moments are mainly contributed by the *Ni* atoms. Furthermore, the direct-indirect band gap transition of monolayer $Ni(OH)_2$ also can be modulated by the biaxial strain. These versatile electronic and magnetic properties of the monolayer $Ni(OH)_2$ open a new door to explore the spintronics in pristine 2D materials.

2. Computational Method

The density functional theory (DFT) calculations were performed by the Vienna Ab Initio Simulation Package (VASP)[36, 37]. Projector augmented-wave (PAW) pseudopotentials[38] were used to account electron-ion interactions. The generalized gradient approximation (GGA) with the PBE functional[39] was used to treat the exchange-correlation interaction between electrons. A vacuum region larger than 15 Å perpendicular to the sheets (along the **c** axis) is applied to avoid the interaction between layers caused by the periodic boundary condition. In our calculations, a kinetic-energy cutoff for plane-wave expansion is set to 500 eV. All the atoms in the unit cell are fully relaxed until the force on each atom is less than 0.005 eV/Å. Electronic energy minimization was performed with a tolerance of 10^{-6} eV. The Brillouin-zone (BZ) sampling is carried out with a 11×11×1 Monkhorst-Pack grids for the 2D sheets. The van der Waals (vdW) interaction is corrected by the DFT-D3 approach[40]. In order to avoid the shortcoming of conventional PBE calculation, the hybrid Heyd-Scuseria-Ernzerhof functional (HSE06)[41, 42] calculations are used to calculate the accurate electronic structure and band gap. The 2×2×1 and 4×4×1 $Ni(OH)_2$ supercells are used for the DFT calculations and phonon dispersion spectrum analysis, respectively. The phonon spectrum is calculated with the PHONOPY package[43] with, which uses the Parlinski–Li–Kawazoe approach[44].

3. Results and Discussion

First of all, the atomic structure and stability of the hexagonal monolayer $Ni(OH)_2$ is examined. The relaxed hexagonal monolayer $Ni(OH)_2$ structure is shown in Figure 1 (a). The monolayer $Ni(OH)_2$ structure belongs to P-3M1(D3D-3) point group symmetry, with Ni atom bonding to six neighboring O atoms, and the H atoms on the top of O atoms. The optimized lattice constant of the monolayer $Ni(OH)_2$ is 3.136 Å, and the Ni-O bond length and O-H bond length are 2.097 Å and 0.971 Å, respectively. To check the thermodynamically stability of the monolayer $Ni(OH)_2$, the phonon frequencies are calculated for all k points in the BZ. The phonon dispersions along the high-symmetry directions in the BZ of the monolayer $Ni(OH)_2$ are presented in Figure 1 (b). The frequencies of all phonon modes in the BZ are positive, which shows the high stability of the monolayer $Ni(OH)_2$ structure.

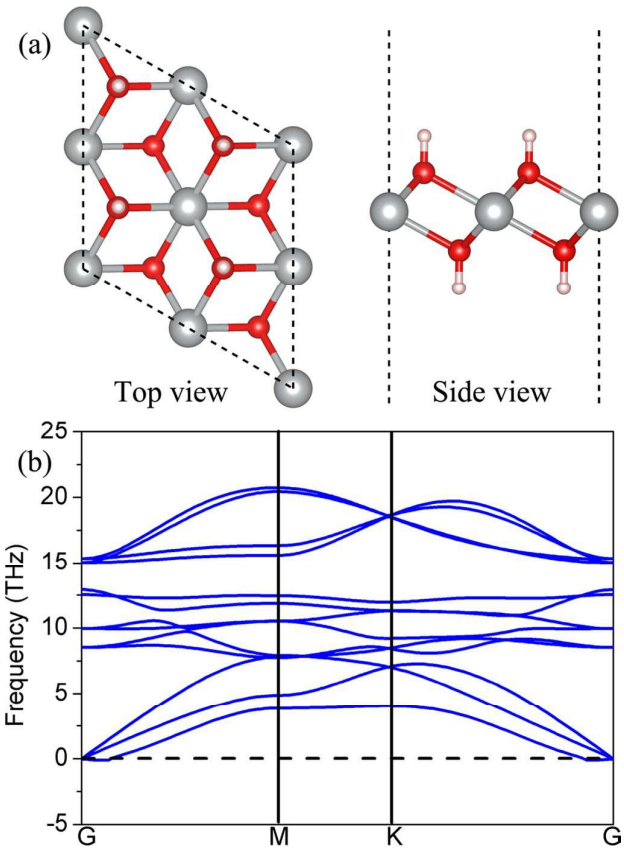

Figure 1 *(a) The relaxed atomic structure of the hexagonal monolayer $Ni(OH)_2$. (b) Phonon dispersions are along the high-symmetry directions in the BZ of monolayer $Ni(OH)_2$. The grey, red and pink balls represent Ni, O and H atoms, respectively.*

After determining the stability, the energies of the monolayer $Ni(OH)_2$ with different magnetic coupling are examined. It is well known that the conventional PBE functional usually underestimates the band gap of semiconductors because of the self-interaction error[45, 46]. The hybrid functional usually gives the more reasonable electronic structure, while it is rather expensive to optimize the geometries to calculate the electronic structure. Thus, in this work, the energy differences between AFM and FM coupling of the monolayer $Ni(OH)_2$ are mainly calculated with PBE, while the electronic structures are analyzed with HSE06 based on the PBE geometries. In order to check the reliability of such approach, another calculation on the pristine monolayer $Ni(OH)_2$ with HSE06 is also carried out. The geometry is fully optimized with HSE06, and then the other properties are further calculated with HSE06. Firstly, the optimized lattice constant of the stress-free $Ni(OH)_2$ is 3.131 Å with HSE06, which is close to the value of 3.136 Å with PBE. Secondly, the energy difference between AFM and FM coupling of the stress-free $Ni(OH)_2$ is -27 meV with HSE06 based on the geometries optimized with HSE06, which is close to the value of -45 meV with PBE. Thirdly, the electronic structures calculated with HSE06 based on both PBE and HSE06 geometries show quite similar results. The band gap of the stress-free monolayer $Ni(OH)_2$ based on the hybrid HSE06 geometry is 3.13 eV, which is quite close to the corresponding ones, 3.15 eV (see Figure 2(a)), calculated

with HSE06 based on the PBE geometries. Such results clearly suggest that the PBE functional can describe well the structure and energy of the monolayer $Ni(OH)_2$. In the following, we mainly discuss the structure and energy calculated with PBE, and the electronic properties calculated with HSE06 based on PBE geometries except we note.

The results show that the most stable magnetic coupling of the pristine monolayer $Ni(OH)_2$ is antiferromagnetic (AFM) coupling, which is 45 and 2586 meV per supercell lower than that of ferromagnetic (FM) and nonmagnetic (NM) coupling, respectively. The ground state band structures of the monolayer $Ni(OH)_2$ with AFM coupling are shown in Figure 2 (a). The band structures show that the pristine monolayer $Ni(OH)_2$ is a semiconductor with a direct band gap of 3.15 eV with HSE06 at the Gamma point. Although the calculated magnetic moment of single Ni atom is 1.733 μ_B, the pristine monolayer $Ni(OH)_2$ does not exhibit any macro magnetic property with AFM coupling between the nearest Ni atoms.

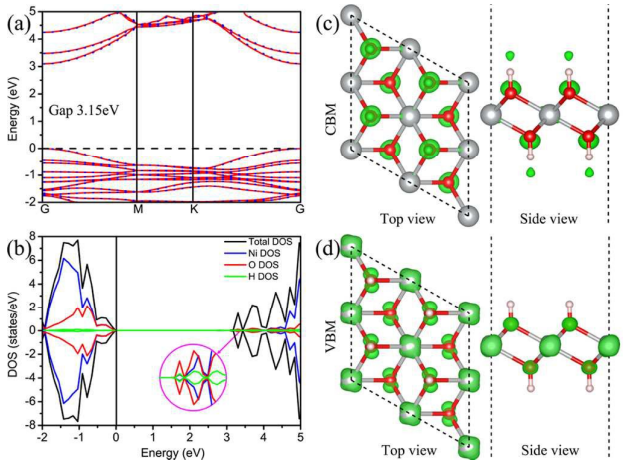

Figure 2 *(a) The band structures of the monolayer $Ni(OH)_2$ with HSE06. The red solid lines and blue dashed lines in the band structures images represent the spin up bands and spin down bands, respectively. (b) The density of states (DOS) of the monolayer $Ni(OH)_2$. The black, red and blue lines represent the total DOS, Ni atoms DOS, O atoms DOS, and H atoms DOS, respectively. (c) and (d) show the partial charge density of the conduction band minimum (CBM) and the valence band maximum (VBM), respectively. The grey, red and pink balls represent Ni, O and H atoms, respectively. The green isosurfaces correspond to the partial charge densities.*

To obtain deeper insight into the electronic structure of the monolayer $Ni(OH)_2$, the density of states (DOS) and projected DOS Ni, O and H atoms are plotted in Figure 2 (b). The projected DOS of Ni, O and H atoms show that the conduction band minimum (CBM) are mainly contributed by the O and H atoms, and while the valence band maximum (VBM) are mainly contributed by the Ni and O atoms. In order to clearly show the distributions of the CBM and VBM in the monolayer $Ni(OH)_2$, the corresponding partial charge densities distributions at the Gamma point are plotted in Figure 2 (c) and (d), respectively. The results show that the CBM at the Gamma point are mainly located on the O atoms and minorly located on the H atoms, and the VBM at the Gamma point mainly located on the Ni atoms and minorly located on the O

atoms.

It is well-known that the strain is widely used to induce and engineer the electronic structures and magnetic property of 2D layered materials[19, 33-35]. Thus, it is desirable to know whether the strain can effectively tune magnetic behavior of the monolayer $Ni(OH)_2$. Here, we investigate the strain effect on the magnetic properties of the monolayer $Ni(OH)_2$ by varying the biaxial strain from -10% to 10%. Figure 3 shows the variation of the energy difference between AFM and FM state (E_{AFM}-E_{FM}) as a function of applied strain, and the positive (negative) values represent that the FM (AFM) is the ground state of the monolayer $Ni(OH)_2$. Interestingly, E_{AFM}-E_{FM} changes from negative to positive under a compressive strain of up to 4%. In that case, a typical FM coupling occurs with 8 μ_B magnetic moments per $Ni(OH)_2$ supercell.

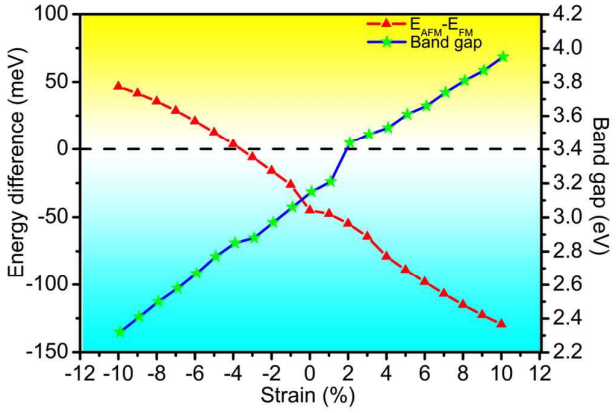

Figure 3 *The calculated energy difference between AFM and FM, E_{AFM}-E_{FM}, and the band gap variation of the monolayer $Ni(OH)_2$ under the different strains.*

The changes of band gaps (green star) under strains are also shown in Figure 3. It is obvious that the band gap of the monolayer $Ni(OH)_2$ drops dramatically under the compressive and tensile strains. The correponding band gaps of the monolayer $Ni(OH)_2$ with 10% compressive strain and 10% tensile strain become 2.32 eV and 3.95 eV, respectively. More importantly, all of the compressive and tensile monolayer $Ni(OH)_2$ remains the property of the direct gap at the Gamma point. These tunable direct band gap in a large range makes the monolayer $Ni(OH)_2$ have potential application in the 2D semiconductor devices.

Finally, the electronic and magnetic properties of the monolayer $Ni(OH)_2$ under two typical strain (10% compressive strain and 10% tensile strain) are examined. As mentioned above, the energy differences between antiferromagnetic (AFM) and ferromagnetic (FM) coupling of the monolayer $Ni(OH)_2$ are mainly calculated with PBE, while the electronic structures are analyzed with HSE06 based on the PBE geometries. In order to check the reliability of such approach on the strain monolayer $Ni(OH)_2$, the hybrid HSE06 functional is employed to examine whether the structure relaxations affect the electronic structure. The typical system of the monolayer $Ni(OH)_2$ under a compressive strain of 10% is used. The geometries are firstly optimized with HSE06, and then the other properties are further calculated. Firstly, the energy differences between AFM and FM coupling of the compressived $Ni(OH)_2$ is

31 meV with HSE06 (the geometries are also fully optimized with HSE06), which is quite close to the value of 47 meV with PBE. Secondly, the electronic structures calculated with HSE06 based on both PBE and HSE06 geometries are quite similar results. The band gap of the compressived $Ni(OH)_2$ based on the hybrid HSE06 geometry is 2.31 eV, which is quite close to the corresponding ones, 2.32 eV, calculated with HSE06 based on the PBE geometries. Such tests further suggest that the approach used above is reliable to examine the electronic properties of the monolayer $Ni(OH)_2$.

The calculated band structures of the monolayer $Ni(OH)_2$ with 10% compressive strain and 10% tensile strain are shown in Figure 4 (a) and (b), respectively. With a 10% compression, the monolayer $Ni(OH)_2$ is a direct semiconductor with a band gap of 2.32 eV. Moreover, both the CBM and VBM are consisted with the spin up bands at the Gamma point. The larger energy difference between the AFM and FM states indicate that the monolayer $Ni(OH)_2$ show strong ferromagnetism with a total magnetic moment of 8 μ_B per supercell. Under 10% tensile strain, the monolayer $Ni(OH)_2$ is an indirect semiconductor with a band gap of 3.95 eV. The total magnetism is zero due to the AFM coupling between the Ni atoms. The corresponding spin density distributions of the monolayer $Ni(OH)_2$ with 10% compressive strain and 10% tensile strain are shown in Figure 4 (c) and (d), respectively. It is clear that the spin densities of the monolayer $Ni(OH)_2$ with 10% compressive strain are mainly localized on the Ni atoms with FM coupling. For the monolayer $Ni(OH)_2$ with 10% tensile strain, the spin densities are also mainly localized on the Ni atoms. However, the monolayer $Ni(OH)_2$ with 10% tensile strain does not exhibit any macro magnetism because of the AFM coupling between the nearest Ni atoms.

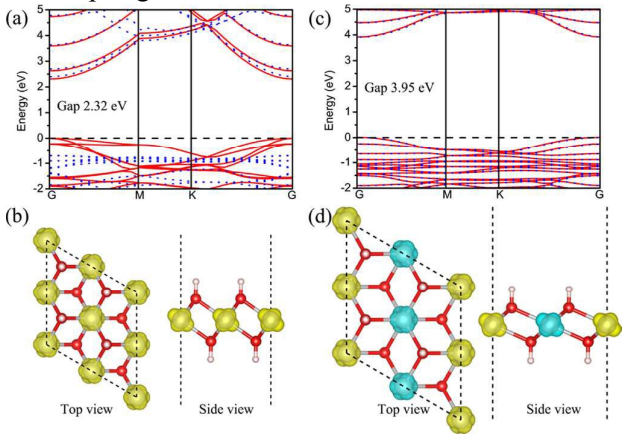

Figure 4 *The band structures of the monolayer $Ni(OH)_2$ under biaxial compressive strain of -10% (a) and biaxial tensile strain of 10% (c). The red solid lines and blue dashed lines represent the spin up and spin down bands, respectively. The corresponding spin density distributions of the monolayer $Ni(OH)_2$ under biaxial compressive strain of -10% (b) and biaxial tensile strain of 10% (d). The grey, red and pink balls represent Ni, O and H atoms, respectively. The yellow and blue-green isosurfaces (the isovalue is 0.3 e / $Å^3$) correspond to the spin up and spin down density, respectively.*

4. Conclusion

Based on first-principle calculations, we demonstrate that the hexagonal monolayer $Ni(OH)_2$ owns versatile electronic properties, which provide a flexible platform to manipulate the band gap and magnetic properties. The phonon dispersion spectrums show that the monolayer $Ni(OH)_2$ is thermodynamically stable. Although the pristine $Ni(OH)_2$ does not display macro magnetism with AFM coupling between two nearest Ni atoms, the monolayer $Ni(OH)_2$ can become FM under a biaxial compressive strain of 4%. And the FM ground state of the monolayer $Ni(OH)_2$ under a biaxial compressive strain has a large magnetic moments of 8 μ_B per supercell. More interestingly, the direct band gap of monolayer $Ni(OH)_2$ also can be tuned by the biaxial strain. The tunable band gap and magnetic properties of the monolayer $Ni(OH)_2$ opens up the tremendous opportunities for the 2D spintronic devices.

Acknowledgments

This work was supported by the National Natural Science Foundation of China (No. 51222212, 11447011), the MOST of China (973 Project, Grant NO. 2011CB922200), the Hunan Provincial Natural Science Foundation of China (No. 2015JJ6013), the Science Foundation of Hengyang Normal University (No. 13B41), the Hunan Provincial Applied Basic Research Base of Optoelectronic Information Technology (No. GD15K04), and the Construct Program for Key Disciplines in Hunan Province.

References

1. K. S. Novoselov, D. Jiang, F. Schedin, T. J. Booth, V. V. Khotkevich, S. V. Morozov and A. K. Geim, *PNAS*, 2005, **102**, 10451-10453.
2. M. Xu, T. Liang, M. Shi and H. Chen, *Chem. Rev.*, 2013, **113**, 3766-3798.
3. A. Du, Z. Zhu and S. C. Smith, *J. Am. Chem. Soc.*, 2010, **132**, 2876-2877.
4. S. Wangmo, R. Song, L. Wang, W. Jin, D. Ding, Z. Wang and R.-Q. Zhang, *J. Mater. Chem.*, 2012, **22**, 23380-23386.
5. F. Li, J. Gao, J. Zhang, F. Xu, J. Zhao and L. Sun, *J. Mater. Chem. A*, 2013, **1**, 8016-8022.
6. P. Thangavelu and B. Jong-Beom, *2D Mater.*, 2015, **2**, 032002.
7. L.-M. Yang, V. Bačić, I. A. Popov, A. I. Boldyrev, T. Heine, T. Frauenheim and E. Ganz, *J. Am. Chem. Soc.*, 2015, **137**, 2757-2762.
8. L.-M. Yang, I. A. Popov, A. I. Boldyrev, T. Heine, T. Frauenheim and E. Ganz, *Phys. Chem. Chem. Phys.*, 2015, **17**, 17545-17551.
9. L.-M. Yang, T. Frauenheim and E. Ganz, *Phys. Chem. Chem. Phys.*, 2015, **17**, 19695-19699.
10. Q. Etienne, R. Frédéric, E. Fabrice, F. Pascal, K. Emmanuel, V. George, G. Feliciano, M.-G. Beatriz, M. Iwan, G. Selmiye Alkan, Y. Ayşe Bayrakçeken, N. Vito Di, T. Alexandr, B. Igor, T. Diana, S. Gotthard, C. Luigi, S. Giorgio, T. Valentina, B. Paolo, P. Grégory, B. Cristina, C. Daniel, S. Gurpreet, R. Teófilo, K. Gunwoo, Y. Wanjing, P. G. Clare and P. Vittorio, *2D Mater.*, 2015, **2**, 030204.
11. K. S. Novoselov, *Science*, 2004, **306**, 666-669.
12. A. H. C. Neto, N. M. R. Peres, K. S. Novoselov and A. K. Geim, *Rev. Mod. Phys.*, 2009, **81**, 109-162.
13. S. David, T. Dinh Van, M. M. D. Simon, G. Martin, W. C. Aron, K. Denis, O. Frank, C.

Jean-Christophe, F. Jaroslav and R. Stephan, *2D Mater.*, 2015, **2**, 022002.

14. R. Stephan, Å. Johan, B. Bernd, C. Jean-Christophe, C. Mairbek, D. Saroj Prasad, D. Bruno, F. Jaroslav, F. Albert, G. Marcos, G. Francisco, G. Irina, S. Christian, S. Pierre, S. Christoph, O. V. Sergio, W. Xavier and W. Bart van, *2D Mater.*, 2015, **2**, 030202.
15. D. D. Awschalom and M. E. Flatte, *Nat. Phys.*, 2007, **3**, 153-159.
16. J. J. Palacios, J. Fernández-Rossier and L. Brey, *Phys. Rev. B*, 2008, **77**, 195428.
17. O. V. Yazyev and L. Helm, *Phys. Rev. B*, 2007, **75**, 125408.
18. Y.-W. Son, M. L. Cohen and S. G. Louie, *Nature*, 2006, **444**, 347-349.
19. Y. Ma, Y. Dai, M. Guo, C. Niu, Y. Zhu and B. Huang, *ACS Nano*, 2012, **6**, 1695-1701.
20. H. Zhang, L.-M. Liu and W.-M. Lau, *J. Mater. Chem. A*, 2013, **1**, 10821.
21. M. Kan, J. Zhou, Q. Sun, Y. Kawazoe and P. Jena, *J. Phys. Chem. Lett.*, 2013, **4**, 3382-3386.
22. M. Kan, S. Adhikari and Q. Sun, *Phys. Chem. Chem. Phys.*, 2014, **16**, 4990.
23. D. Gao, Q. Xue, X. Mao, W. Wang, Q. Xu and D. Xue, *J. Mater. Chem. C*, 2013, **1**, 5909.
24. K. Watanabe, T. Kikuoka and N. Kumagai, *J. Appl. Electrochem.*, 1995, **25**, 219-226.
25. D. E. Reisner, A. J. Salkind, P. R. Strutt and T. D. Xiao, *J. Power Sources*, 1997, **65**, 231-233.
26. H. Wang, H. S. Casalongue, Y. Liang and H. Dai, *J. Am. Chem. Soc.*, 2010, **132**, 7472-7477.
27. J. Yan, Z. Fan, W. Sun, G. Ning, T. Wei, Q. Zhang, R. Zhang, L. Zhi and F. Wei, *Adv. Func. Mater.*, 2012, **22**, 2632-2641.
28. S. Ida, D. Shiga, M. Koinuma and Y. Matsumoto, *J. Am. Chem. Soc.*, 2008, **130**, 14038.
29. G. Li, X. Wang, H. Ding and T. Zhang, *RSC Adv.*, 2012, **2**, 13018.
30. J. D. Rall, M. S. Seehra and E. S. Choi, *Phys. Rev. B*, 2010, **82**, 184403.
31. P. Hermet, L. Gourrier, J. L. Bantignies, D. Ravot, T. Michel, S. Deabate, P. Boulet and F. Henn, *Phys. Rev. B*, 2011, **84**, 235211.
32. S. A. Wolf, D. D. Awschalom, R. A. Buhrman, J. M. Daughton, S. von Molnár, M. L. Roukes, A. Y. Chtchelkanova and D. M. Treger, *Science*, 2001, **294**, 1488.
33. Y. Zhou, Z. Wang, P. Yang, X. Zu, L. Yang, X. Sun and F. Gao, *ACS Nano*, 2012, **6**, 9727-9736.
34. H. Guo, N. Lu, L. Wang, X. Wu and X. C. Zeng, *J Phys. Chem. C*, 2014, **118**, 7242-7249.
35. Z.-K. Tang, X.-B. Li, D.-Y. Zhang, Y.-N. Zhang and L.-M. Liu, *J Mater. Chem. C*, 2015, **3**, 3189-3197.
36. G. Kresse and J. Furthmüller, *Phys. Rev. B*, 1996, **54**, 11169.
37. G. Kresse and J. Furthmüller, *Comput. Mater. Sci.*, 1996, **6**, 15.
38. G. Kresse and D. Joubert, *Phys. Rev. B*, 1999, **59**, 1758.
39. J. P. Perdew, K. Burke and M. Ernzerhof, *Phys. Rev. Lett.*, 1996, **77**, 3865.
40. S. Grimme, J. Antony, S. Ehrlich and H. Krieg, *J. Chem. Phys.*, 2010, **132**, 154104.
41. J. Heyd, G. E. Scuseria and M. Ernzerhof, *J. Chem. Phys.*, 2003, **118**, 8207-8215.
42. J. Heyd, G. E. Scuseria and M. Ernzerhof, *J. Chem. Phys.*, 2006, **124**, 219906.
43. A. Togo, F. Oba and I. Tanaka, *Phys. Rev. B*, 2008, **78**, 134106.
44. K. Parlinski, Z. Q. Li and Y. Kawazoe, *Phys. Rev. Lett.*, 1997, **78**, 4063-4066.
45. M. Hybertsen and S. Louie, *Phys. Rev. Lett.*, 1985, **55**, 1418-1421.
46. M. Hybertsen and S. Louie, *Phys. Rev. B*, 1986, **34**, 5390-5413.